



1 **Evolution of Maud Rise Polynya during the last 250 years – a 2 multiproxy ice core reconstruction from coastal Dronning Maud 3 Land, Antarctica**

4 Rahul Dey^{1,2}, Chavarukonam M. Laluraj¹, Kenichi Matsuoka³, Ashish Paiguinkar¹, Bhikaji L
5 Redkar¹ and Meloth Thamban¹

6 ¹National Centre for Polar and Ocean Research (NCPOR), Ministry of Earth Sciences, Vasco da Gama, Goa
7 403804, India

8 ²Physics of Ice, Climate and Earth, Niels Bohr Institute, University of Copenhagen, Copenhagen N 2200,
9 Denmark

10 ³Norwegian Polar Institute, Framsentret, Postboks 6606, Langnes, 9296 Tromsø, Norway

11 *Correspondence to:* Rahul Dey (rdey1801@gmail.com)

12 **Abstract**

13 Open ocean polynyas drive deep ocean convection, influencing regional carbon and heat
14 budgets, which in turn influence the ocean circulation and overall climate of Antarctica. The
15 Maud Rise Polynya (MRP), also known as the Weddell Polynya, is one such polynya that forms
16 in the Southern Ocean during early spring or winter months. The extensively studied MRP
17 opening, which occurred during 2016-2017 and 1974–1976, triggered intense convection,
18 ventilating heat from the deep ocean and modifying water mass properties. However, polynya
19 evolution beyond the satellite era remains poorly understood. Here, we develop a polynya index
20 using multiple proxy records from an ice core in coastal Dronning Maud Land, East Antarctica.
21 Our approach—integrating records of snow accumulation, $\delta^{18}\text{O}$, deuterium excess, Na flux,
22 and Na/SO₄ ratios—enhances polynya reconstruction, thereby overcoming the limitations of
23 single-proxy methods. The index replicates the 1974–1976 polynya and extends the record to
24 1774, revealing three major events comparable to the 1974–1976 great polynya event, in the
25 past 250 years, totalling 47 polynya years. We identified distinct clusters of polynya activity,
26 possibly corresponding to a specific combination of atmospheric circulation patterns and
27 oceanographic preconditioning for MRP development. This study offers a long-term
28 perspective on MRP variability, providing insights into its drivers and climate-related impacts.



29 1. Introduction

30 Open ocean polynyas represent one of the most dynamic and influential features in the
31 Southern Ocean system, serving as critical regulators of heat and gas exchange between the
32 ocean and atmosphere. These persistent areas of open water within the sea ice cover act as
33 windows through which complex oceanographic and atmospheric processes interact,
34 influencing global ocean circulation, carbon cycling, and climate patterns (Bennetts et al.,
35 2024; The SO-CHIC consortium, 2023; Zheng et al., 2021). The significance of polynyas
36 extends beyond their immediate vicinity, influencing deep-water formation, marine ecosystem
37 dynamics, and global climate processes. In the Southern Ocean, polynyas manifest in two
38 distinct forms: (1) coastal polynyas, which form along the Antarctic margin through
39 mechanical forcing by katabatic winds, and (2) open-ocean polynyas, which develop hundreds
40 of kilometres offshore through complex thermodynamic processes. While coastal polynyas
41 occur regularly and have been extensively studied (Arrigo and van Dijken, 2003; Årthun et al.,
42 2013; Jacobs et al., 1979; Visbeck et al., 1996; Xu et al., 2023), open-ocean polynyas represent
43 rare but profoundly influential events that can significantly impact global ocean circulation
44 patterns. The Maud Rise Polynya (MRP), also known as Weddell Polynya, occurring over the
45 Maud Rise seamount in the eastern Weddell Sea (Fig. 1), is the most enigmatic open-ocean
46 polynya in the Southern Ocean (Holland, 2001). First documented through satellite
47 observations in the 1970s, the MRP reached its largest extent during the winter and early spring
48 months from 1974 to 1976, exceeding 300,000 km² at its peak (Carsey, 1980; Zwally et al.,
49 1985). This event drove intense ocean convection, reaching depths of over 3000 meters, and
50 fundamentally altered water mass properties throughout the region, influencing global ocean
51 circulation patterns (Gordon and Comiso, 1988).

52 Following this dramatic episode, the Maud Rise region has exhibited intermittent
53 polynya activity, typically manifesting as halos of reduced sea ice concentration (Lindsay et
54 al., 2004; McHedlishvili et al., 2022). However, the phenomenon garnered renewed attention
55 when a large polynya exceeding 40,000 km² reappeared during the two winters of 2016 and
56 2017 (Jena et al., 2019). Early polynya studies focused primarily on documenting polynya
57 occurrence and extent through satellite imagery (Carsey, 1980; Comiso and Gordon, 1987;
58 Zwally et al., 1985), while more recent works have attempted to unravel the complex
59 mechanisms controlling polynya formation and maintenance (de Lavergne et al., 2014; Wilson
60 et al., 2019). Satellite observations have revealed that open-ocean polynya formation often



61 follows a characteristic pattern, beginning with the appearance of small-scale openings that can
62 rapidly expand under favourable conditions, such as wind-driven upwelling (de Lavergne et
63 al., 2014; Jena et al., 2019), baroclinic instabilities (Akitomo, 2006; Campbell et al., 2019),
64 and deep warm water intrusions (Gulk et al., 2024; Heuzé et al., 2021). However, the precise
65 triggers initiating this process remain incompletely understood, because the relative importance
66 of these processes likely varies temporally and may be interconnected (Campbell et al., 2019;
67 McPhee, 2003; Narayanan et al., 2024), and also because large polynyas openings are rare and
68 satellite-based observations range only for the past few decades, limiting the observational
69 opportunity. Similarly, model-based assessments are limited in their ability to understand
70 polynya formation in the weakly stratified Southern Ocean (Heuzé et al., 2013; Sallée et al.,
71 2013). This modelling challenge hampers our ability to assess both the role of polynyas in
72 natural climate variability and their potential responses to future climate change.

73 To obtain longer polynya records, Goosse et al. (2021) examined surface mass balance
74 (SMB) records reconstructed from six ice cores and two automatic weather stations. In these
75 records, they found that increased snowfall during the 2016-17 MRP opening assumed that this
76 had also occurred in past MRP opening periods. Their study constructed a polynya index using
77 two data assimilation approaches and one statistical method to reconstruct historical climate
78 states based on SMB reconstruction from ice cores. Their study found multiple polynya
79 openings since 1250 CE, but observed that large polynya openings are rare. However, they rely
80 only on snow accumulation records, which can be influenced by many factors other than
81 polynya occurrences. The polynya signal in their ice-core SMB records is also weak compared
82 to natural atmospheric variability, making it difficult to distinguish polynya-induced anomalies
83 from SMB caused by other climatic fluctuations. The short instrumental record from automatic
84 weather stations prevents a robust calibration of polynya reconstructions, increasing the risk of
85 false positives (unrelated high snowfall events misinterpreted as polynya activity) and false
86 negatives (missed polynya events). Additionally, the ice-core and instrumental records they
87 used were collected from a large region, including the Weddell Sea sector and the ice sheet
88 inland, where the surface elevation exceeds 2000 m a.s.l., which can hardly reflect changes in
89 the vapour sources in the MRP regions directly (Fig. 1).

90 To overcome the limitations of the previous study, we develop a novel, multi-proxy
91 approach to reconstruct past MRP activity using a high-resolution ice core, IND-36/9, from



92 Djupranen Ice Rise in coastal Dronning Maud Land. While polynya opening results in
93 increased heat and moisture exchange, the polynya years, characterised by a decrease in sea ice
94 cover, also result in increased sea salt production. These signatures can be carried to the coastal
95 region of Antarctica and deposited in the low-elevation ice shelves and ice rises. The back-
96 trajectory analysis (Section x) clearly indicates the direct atmospheric link between MRP and
97 the IND-36/9 core site (Fig. 1). Our ice core site is situated within ~1000 km of the typical
98 MRP location, close enough to potentially capture atmospheric signatures transported from
99 polynya formation near the Maud Rise. By combining records of snow accumulation, water
100 isotopes, and major ion concentrations, we aim to provide a more robust reconstruction of
101 polynya activity. This approach leverages the strengths of selecting an idea core site and
102 employing multiple proxies to overcome the limitations of single-proxy reconstructions,
103 thereby capturing the complex signatures of polynya events that extend beyond the last few
104 decades, when satellite and instrumental records are available.

105 **2. Study Area and Methods**

106 **2.1. Study area**

107 The DML coast is characterised by distinct topographic features like ice rises having
108 associated local ice flow, climate regime and SMB variability (Drews et al., 2015; Goel et al.,
109 2017; Lenaerts et al., 2014; Matsuoka et al., 2015; Pratap et al., 2022; Rignot et al., 2019). As
110 part of the Indo-Norwegian project MADICE, an ice core was drilled on the summit of the
111 Djupranen Ice Rise (70.18° S, 9.18° E; elevation 321 m a.s.l.), at the western margin of the
112 Nivlisen Ice Shelf in coastal Dronning Maud Land (DML), East Antarctica (Fig. 1). Our site
113 survey found that this ice rise summit has been at the current position at least in the past few
114 millennia (Pratap et al., 2022). This location also offers several advantages for polynya
115 reconstruction: its high SMB allows annual layer counting (Dey et al., 2023) and its coastal
116 proximity may provide sensitivity to maritime signals (Ejaz et al., 2021; Wauthy et al., 2024),
117 while its elevation causes insignificant surface melt and local noise while maintaining regional
118 signal strengths (Dey, 2023). Its position is also within primary atmospheric transport pathways
119 from the Maud Rise region (Fig. 1).



120 **2.2. Ice core: from the field to the laboratory**

121 The drill site of the Djupranen ice rise was located at its summit, based on analysis of
122 satellite altimetry data and satellite image analysis, followed by an ice-penetrating radar survey
123 (Pratap et al., 2022). The radar survey also revealed Raymond arches, indicative of a relatively
124 stable summit position in the past (Goel et al., 2020). The ice core was drilled using an
125 electromechanical ice core drilling system (Model D2, GeoTec, Japan). Over nine days, a 122
126 m ice core (IND 36/B9; hereafter IND36/9) was retrieved. The drilled ice core sections were
127 sealed in high-density polyethylene core bags, packed in expanded polypropylene boxes, and
128 stored in a reefer container at -20°C until their transport to the National Centre for Polar and
129 Ocean Research (NCPOR), Goa, India, where samples were stored in the in-house Ice Core
130 Laboratory maintained at -20°C . The ice cores were processed in the -15°C core processing
131 facility at NCPOR. The cores were initially cut into 3.5 cm thick, 10 cm wide slabs for line
132 scanning and then subsequently sub-sampled at 5 cm resolution for stable isotope and chemical
133 analysis. The samples for chemical analysis were cut into cuboids; the three dimensions of the
134 samples were measured using a calliper and weighed using a weighing balance. The density
135 for the samples was calculated as mass divided by the volume of each sample. The error in
136 measuring the sample dimensions was ± 0.5 mm, while the weighing balance's uncertainty was
137 ± 0.1 g for measurements up to 100 g. As a result, the density measurements have a propagated
138 uncertainty of 5%.

139 Major inorganic anions (Cl^- , SO_4^{2-} , MSA^- and NO_3^-) and cations (Na^+ , NH_4^+ , K^+ , Mg^{2+} ,
140 and Ca^{2+}) were measured in the samples using an ICS 5000+ ion chromatograph (Thermo
141 Dionex) equipped with a conductivity detector. Anions were separated on an AS11 (2 mm)
142 column with potassium hydroxide as eluent and an AG11 (2 mm) guard column with AERS
143 500, 2 mm suppressor. Cations were separated on a CS17 (0.4 mm) capillary column with a
144 methane sulphonic acid as the eluent and the CG17 (0.4 mm) capillary guard column with a
145 CCES 300 capillary suppressor. A 10 mg/L stock solution of Na^+ , NH_4^+ , K^+ , Ca^{2+} , and Mg^{2+}
146 was mixed and then diluted with MiliQ ultrapure water to prepare standards for cation
147 exchange chromatography. The anion standards were prepared from 10 ppm stock solutions of
148 MSA^- , Cl^- , SO_4^{2-} , and NO_3^- . The dilutions were conducted volumetrically and were freshly
149 prepared within a few days of each run, ranging from 5 ppb to 1 ppm. Eight standards were
150 selected from this range for calibration. Before analysis, the ice core samples were melted in a
151 Class 100 clean room. The analytical precision for all ions was better than 10%.



152 The ice core samples were analysed for oxygen and hydrogen isotopic ratios at NCPOR
153 using a Triple Isotope Water Analyser (TIWA-45EP from Los Gatos Research, USA), which
154 works on the principle of off-axis integrated cavity output spectroscopy (OA-ICOS). The
155 melted ice core samples were introduced into the TIWA-45EP without sample conversion
156 through a PAL HTC-xt auto-injector (CTC Analytics) equipped with a heated (\approx approximately
157 85 °C) injector block (LGR) (Berman et al., 2013). Using a Hamilton 1.2 μ L, zero-dead-volume
158 syringe, samples were injected into the injector block and evaporated for direct isotope
159 analysis. Measurements were completed at a speed of \sim 90 s per individual injection. To
160 eliminate sample-to-sample memory, a total of nine injections were made, with the first three
161 being discarded for analysis. The last six injections were averaged to produce a single, high-
162 throughput (HT) sample measurement. One commercially available working standard from
163 LGR1C and two in-house laboratory standards (CDML1 and HL1) with known isotopic
164 composition, spanning the entire range of our sample measurements (-46.19 ‰ to -19.49 ‰
165 for $\delta^{18}\text{O}$ and -362.85 ‰ to -154.0 ‰ for δD) were analysed routinely as reference waters after
166 every five ice core samples to check the instrument performance. Laboratory standards are
167 calibrated on the VSMOW/SLAP scale. The external precision obtained using our laboratory
168 standards (CDML1 and HL1) for $\delta^{18}\text{O}$ was ± 0.046 ‰ and ± 0.068 ‰, respectively, and for δD
169 was ± 0.32 ‰ and ± 0.23 ‰ (1σ standard deviation) for 30 samples. Replicate analyses
170 performed based on ten samples yield repeatability of ± 0.76 ‰ for δD and ± 0.09 ‰ for $\delta^{18}\text{O}$.
171 All the raw instrumental OA-ICOS data were processed in the LGR post-analysis software.
172 Any measured injection with water number density outside the manufacturer's suggested range
173 of $2\text{--}4.5 \times 10^{16} \text{ H}_2\text{O molecules/cm}^3$ was discarded. Injections with incomplete evaporation were
174 detected by examining the standard deviation of the measured water number density (σ_{nmeas}) as
175 reported by the instrument (Berman et al., 2013). Processed raw data directly gives $\delta^{18}\text{O}$ and
176 δD , which are further used to calculate deuterium excess [$\text{d-excess} = \delta\text{D}_{\text{ice}} - 8 \times \delta^{18}\text{O}_{\text{ice}}$].

177 **2.3. Chronology development**

178 The chronology of the IND36/9 core is based on a multiproxy approach involving
179 annual layer determination from the stratigraphy of $\delta^{18}\text{O}$, major ions, and pixel intensity data
180 from the line scanner, following Dey et al. (2023). The core has experienced limited surface
181 melt, with annual melt proportion varying between 0 and 4.4%, with a median melt proportion
182 of 0.25% (Dey et al., 2023). Since diffusion in the firn attenuates high-frequency water-



183 isotope information in ice cores (The Firn Symposium team, 2024), even in high accumulation
184 sites of coastal Antarctica (Mahalinganathan et al., 2022), we diffusion-corrected our water
185 isotope records following Jones et al. (2023) as detailed in the supplementary materials (Fig.
186 S1). The shift in seasonal peaks in our corrected record is less than 5 cm, which falls within
187 the sampling interval of 5 cm and is therefore insignificant in affecting the accuracy of the
188 chronology.

189 A five-point smoothing was applied to the pixel intensity data to simplify annual layer
190 counting and reduce noise in the record. We also used age tie points of known volcanic
191 eruptions identified from non-sea-salt sulphate (nssSO₄) peaks, as well as the tritium bomb
192 peak of 1962. Volcanic indicators (nssSO₄) have been used to identify specific, dated volcanic
193 eruptions, allowing us to reduce the uncertainties resulting from the relative dating procedure.
194 However, unambiguous eruption identifications are challenging in ice cores from coastal
195 regions, where the nssSO₄ background signals are commonly highly variable due to the
196 proximity of the ocean and ocean-related MSA products (Philippe et al., 2016).

197 A preliminary chronology was obtained from the annual counts, which was then
198 refined using the nssSO₄ peaks (Fig. 2) from the well-established volcanic eruptions of
199 Pinatubo (1991), El Chichon (1982), Agung (1963), Cerro Azul (1932), Santa Maria (1902),
200 Krakatoa (1882), Cosiguina/Babuyan (1834), Tambora (1815) and unknown volcanic
201 eruption (1809). Similar to Dey et al. (2023), we refined the chronology between the volcanic
202 and Tritium tie points using the StratiCounter algorithm (Winstrup et al., 2012). The manual
203 counts provide a basic framework from which StratiCounter develops and refines its statistical
204 characterisation of annual layers, enabling adaptation to varying layer properties with depth
205 (Winstrup et al., 2012). To minimise reliance on initial manual inputs, we conducted multiple
206 iterations using refined layer templates derived from previous algorithm outputs. The
207 chronology of the IND36/9 ice core provides a robust temporal framework that extends back
208 to 1774 CE at a depth of 122m (Fig. 3).

209 **2.4. Satellite-based polynya metrics**

210 We followed Heuzé et al. (2021) to define the "polynya-prone" region of the Weddell
211 Sea (6°W to 12°E, 68°S to 60°S, approximately 600 km x 900 km), focusing on the winter and
212 early spring months (June 1 to October 31). This region was selected based on historical



213 observations of polynya formation and its significance in Antarctic bottom water production
214 (Campbell et al., 2019; Heuzé et al., 2021). Polynya activity was quantified using two
215 independent metrics derived from satellite data. These metrics complement each other to
216 provide a comprehensive assessment of polynya dynamics.

217 The first metric, Polynya Days, represents the annual count of days (between June 1
218 and October 31) with sea ice concentration below 60% in our study zone. This threshold was
219 determined through sensitivity analysis of satellite imagery and validation against in situ
220 observations from previous studies (Heuzé et al., 2021). Sea ice concentration data were
221 derived from passive microwave measurements using the NASA Team algorithm (Comiso and
222 Nishio, 2008), which has demonstrated robust performance in discriminating between open
223 water and sea ice in polar regions. The second metric, Cumulative Polynya Area, measures the
224 total extent of all polynya occurrences within a year (June 1 to October 31). This metric was
225 calculated by summing the daily polynya areas, defined as contiguous regions with sea ice
226 concentration below the 60% threshold. The combination of these metrics allows us to
227 characterise both the temporal persistence and spatial extent of polynyas, providing insights
228 into their formation mechanisms and potential impact on regional oceanographic processes.

229 **2.5. Air mass trajectory modelling**

230 The HYbrid Single-Particle Lagrangian Integrated Trajectory (HYSPLIT) model,
231 developed by the NOAA Air Resources Laboratory (ARL), provides a means of generating
232 back trajectories to identify the source of moisture uptake for precipitation (Markle et al.,
233 2012). We used HYSPLIT version 5.3 for back trajectory computations, initialized with
234 conditions from the 2.5 by 2.5-degree resolution NCEP/National Center for Atmospheric
235 Research (NCAR) reanalysis data for the period 1948 to 2016. Forward trajectories were run
236 for 240 hours (10 days), initialised every hour, starting over the polynya-prone region of the
237 Weddell Sea. Groups of forward trajectories were computed with initial altitudes of 100, 200,
238 300, 400, and 500 meters above ground level, and in all cases, the vertical velocity from the
239 meteorological data was used as the input for vertical motion.

240 We calculated trajectory density from multiple trajectories using HYSPLIT (Miller et
241 al., 2002), because individual trajectories are highly sensitive to meteorological uncertainties,
242 turbulence, and small initial condition variations, often leading to misleading or unreliable



243 airflow pathways and potential position errors of up to 20% of the distance travelled. It also
244 aids in discriminating between local circulation patterns and regional-scale flow features
245 (Dorling and Davies, 1995) and has been previously applied to interpret polar ice core
246 paleoclimate records (Dixon et al., 2012; Ejaz et al., 2021; Neff and Bertler, 2015). We
247 calculated air mass transport densities for each year 1979 – 2016 from the HySPLIT output.
248 The trajectory endpoints in each equal-area (1 by 1 degree) oceanic pixel were summed and
249 divided by the total number of air mass trajectories.

250 **3. Results**

251 **3.1. Identification of polynya years in satellite data**

252 Satellite imageries are crucial for polynya studies as they provide continuous, high-
253 resolution observations of sea ice dynamics, allowing researchers to monitor polynya
254 formation, extent, and variability over time. Satellite observations spanning four decades reveal
255 distinct periods of polynya activity in the Weddell Sea region since 1979 (Fig. 4). The most
256 notable and well-documented event occurred during 1974-1976, when the polynya reached an
257 exceptional size of 300,000 km² (Carsey, 1980). This event, often referred to as the Great
258 Weddell Polynya, represented a significant perturbation to the regional ocean-atmosphere
259 system and has served as a benchmark for subsequent polynya observations. Following this
260 major event, several smaller polynyas and polynya-like features ("halos") have been observed
261 during the late 1980s to early 1990s and early 2000s (Heuzé et al., 2021). The two independent
262 metrics used for polynya detection—Polynya Days and Cumulative Area—reveal distinct but
263 complementary temporal patterns. This dual-metric approach enables a more comprehensive
264 understanding of polynya dynamics than either metric alone could provide. While the
265 magnitudes of these metrics do not exhibit direct correlation ($r = 0.42$, $p < 0.01$), both metrics
266 successfully identify known major polynya/halo events between 1979 and 2016, and provide
267 unique insights into their temporal and spatial characteristics. The Polynya Days metric
268 effectively captures persistent small-scale features, while the Cumulative Area metric better
269 represents brief but large openings. While the record of polynya openings from satellite
270 imagery provides crucial insights, their influence on coastal Antarctic ice cores could depend
271 majorly on atmospheric transport.



272 **3.2. Air mass transport patterns**

273 We use forward air trajectory analysis to examine the transport pathways and determine
274 whether polynya-derived signals can reach and be recorded in the ice cores. This approach
275 allows us to trace the path of air masses from the polynya-prone area to potential ice core sites,
276 providing insight into which locations are most likely to capture polynya signals. Forward
277 trajectory analysis reveals consistent and well-defined transport pathways from the Maud Rise
278 region to coastal Dronning Maud Land (Fig. 5). Frequency analysis indicates that our study
279 site receives approximately 2% of all trajectories originating from the MRP region, a
280 statistically significant proportion ($p < 0.001$) that indicates reliable capture of polynya-related
281 atmospheric signals. This percentage remains relatively stable across different seasons and
282 years, suggesting a robust atmospheric connection between the source and deposition regions.
283 The trajectory density analysis indicates that our ice core location falls within a primary
284 atmospheric transport corridor originating from the MRP region. This corridor exhibits
285 enhanced stability during the winter months when polynya formation typically occurs.
286 However, trajectory calculations are susceptible to significant spatial error of 15 – 30% of
287 distance travelled (Draxler, 2008). Therefore, a combination of forward and backward
288 trajectories would provide a better overview of the travel pathways. Our back-trajectory
289 analysis (Fig. 6) further confirms the findings from the forward trajectory patterns, showing
290 trajectories originating from the polynya-prone region influencing our ice core site. Trajectory
291 analysis of the transport pathways, therefore, confirms that winds can carry polynya-derived
292 signals from the open water to our study site and preserve them in the ice core records,
293 regardless of polynya presence.

294 **3.3. Development of the polynya index**

295 *3.3.1. Ice core record and proxy selection*

296 The ice core proxy dataset from 1774 to 2016 exhibits distinct variability across all
297 measured properties. We choose five major proxies for developing our polynya index: sea-salt
298 sodium (ssNa), deuterium excess (d-excess), $\delta^{18}\text{O}$, snow accumulation, and the Na/SO₄ ratio
299 (Fig. 7a). Sodium concentration ranges from a low of 19.10 to 218.64 ppb, with a mean value
300 of 89.87 ppb. Some periods show sustained higher values, such as the late 1700s and early
301 1800s, while others, including the late 19th and 20th centuries, display more variable levels.



302 D-excess varies between -1.83 to 10.75‰, with a mean of 4.31‰, showing notable peaks in
303 the late 19th century and sharp declines in the early 20th century. $\delta^{18}\text{O}$ values fluctuate between
304 -21.64 to -15.65‰, with a mean of -17.85‰, displaying alternating periods of enrichment and
305 depletion, including a gradual decline over recent decades. Annual snow accumulation ranges
306 from 0.12 to 0.83 m w.e., with a mean of 0.39 m w.e., exhibiting distinct fluctuations, including
307 lower values in the early 20th century and a more variable pattern in recent decades. The
308 Na/SO₄ ratio ranges from 0.02 to 1.31, with a mean of 0.42, exhibiting periodic fluctuations
309 throughout the dataset.

310 Our polynya index incorporates the five selected parameters, each chosen based on
311 established physical mechanisms that link polynya formation to specific signatures in ice core
312 records. The opening of a polynya results in increased heat and moisture exchange between the
313 warm, open water and the cold air. Therefore, during polynya years (decrease in the sea ice
314 cover), there is also an increase in local precipitation in the Weddell Sea region (Moore et al.,
315 2002) and resultant snow accumulation further inland (Goosse et al., 2021). The water isotope
316 ratios of precipitation are often related to temperature at the precipitation site (Ejaz et al., 2022;
317 Naik et al., 2010) and the distance of transport (Goursaud et al., 2017; Klein et al., 2019), and
318 the pattern of annual mean water isotopes of precipitation associated with polynya formation
319 would relatively be similar to that for increased temperature from the heat exchange due to
320 polynya opening and shorter transport distance, especially over a coastal site. Extensive open
321 water polynyas can also act as a large factory for sea ice production, comparable to the
322 production of the largest coastal polynyas (Zhou et al., 2023). Previous studies have
323 demonstrated that the surface of fresh sea ice, including frost flowers, is the major source of
324 sea salt to the Antarctic, and the production of frost flowers is controlled by the amount of new
325 sea ice production (Wolff et al., 2003). Therefore, the formation of large open-ocean polynyas
326 would lead to an increased supply of sea salt sodium to the ice core site.

327 Additionally, Sulphate (SO₄) fractionation during freezing of seawater (ice) is another
328 well-known process to characterise sea ice coverage (Richardson, 1976). It is driven by the
329 crystallisation of Na₂SO₄·10H₂O (mirabilite) occurring at temperatures below -8.2°C. Since the
330 salt crystals are associated with the ice lattice, the remaining brine becomes increasingly
331 depleted in SO₄ (and to a lesser extent in Na) as it progresses below this critical temperature.
332 This process, therefore, increases the Na/SO₄ ratio of the sea salt source relative to bulk



333 seawater by preferentially removing sulphate ions (Wagenbach et al., 1998). Since this process
334 only occurs at temperatures below -8.2 °C, temperatures not encountered at the summer ocean
335 surface, but frequently encountered at the winter sea ice surface (Levine et al., 2014). The
336 anomalously high Na/SO₄ ratio can be used as an indicator of sea salt sourced from the
337 production of fresh sea ice at the polynyas.

338 *3.3.2. Development of the integrated polynya index*

339 Our ice core record shows an anomalous increase in all proxy records during the
340 prominent polynyas of 1964 and 1974–1976 (Fig. 7a). However, in the case of the transient
341 polynyas and halos in more recent years, the relative changes are weaker but still identifiable.
342 This could be due in part to the inherent complexity of air-ocean interactions and transportation
343 processes, as well as the uncertainty associated with the measurements and chronology of the
344 ice core. Therefore, to develop a more robust proxy, rather than using the proxies individually,
345 we derive a multi-proxy index to quantify the likelihood of polynya occurrence more
346 accurately.

347 The polynya index is defined using anomalous changes in snow accumulation, $\delta^{18}\text{O}$,
348 deuterium excess, Na_{flux}, and Na/SO₄ ratio as possible indicators of polynya activity. We used
349 Monte Carlo simulations to account for uncertainties associated with these individual proxies
350 and ultimately to constrain better the influence of these uncertainties on the multi-proxy
351 polynya index. This is because individual measurement uncertainties are independent of
352 chronological uncertainties. We run ten thousand simulations to minimise statistical bias and
353 define background data as the sum of a 30-year running median (RM) and two times of median
354 absolute deviations (MAD). A polynya year (a year when a polynya activity is recorded) is
355 defined as a year in which the polynya index exceeds the likelihood threshold (0.6, 0.8, or 1).
356 The polynya index is, therefore, an indicator of polynya occurrence from ice core observations
357 and not a measure of the absolute extent or duration of the polynya events.

358 **3.4 Past Maud Rise Polynya activity**

359 Our ~250-year reconstruction reveals complex and significant temporal variability in
360 polynya occurrence, shedding new light on the long-term behaviour of the Maud Rise Polynya
361 (MRP). We identified forty-seven distinct polynya years from 1774 to 2016 (Fig. 7b); however,
362 the period from 1920 to 1950 was the longest interval without significant polynya activity in



363 our record. The 1830s were the most active decade, with seven polynya years recorded between
364 1830 and 1840. This high frequency of events suggests that atmospheric and oceanic conditions
365 during this period were highly conducive to polynya formation. Similar clusters occurred in
366 the 1880s, with five polynya years, and in the 1970s, with four polynya years, including the
367 well-documented 1974–1976 sequence (Fig. 7b). These clusters suggest potential links to large-
368 scale climate oscillations or recurring oceanographic conditions that favour polynya
369 development. The reconstruction also identifies two past events (1833 – 1884 and 1911) that
370 produced index values comparable to or exceeding those of the well-documented 1974–1976
371 polynya. The high index values for these events likely indicate that they were large-scale and
372 persistent openings; however, exact quantification of the polynya extent is beyond the scope of
373 this study.

374 **4. Discussion**

375 **4.1. Performance of the new polynya index**

376 We compared our polynya index with those from Goosse et al. (2021) and found that
377 all major polynyas identified in their study over the common time period are also identified in
378 this study. This provides a degree of validation for both approaches, suggesting that they are
379 capturing similar large-scale polynya events. However, our index shows enhanced sensitivity
380 to polynya formations, identifying the polynya occurrence of 1964, even though with a low
381 likelihood. This low likelihood of the 1964 polynya is possibly due to the lower persistence as
382 compared to the well-documented events during 1974 – 1976 (Meier et al., 2013). Furthermore,
383 our index shows better performance in identifying transient polynyas and halos, which were
384 missed in the reconstruction by Goosse et al. (2021). These shorter-lived or less intense polynya
385 events, while not as dramatic as major openings, play a crucial role in regional oceanography
386 and climate dynamics. Their detection provides a more comprehensive picture of polynya
387 activity over time.

388 Visual inspection shows that some years show synchronised peaks across the indices
389 from the two studies, with leads/lags associated with the timescale of the ice cores (Fig. 8).
390 However, some peaks are present in our polynya index which are absent/muted in Goosse et
391 al. (2021). This discrepancy between the two records is possibly due to the selection of ice core
392 sites used for calculating the polynya index. Our analysis of air mass transport frequency from



393 the MRP regions shows a sink in the coastal regions of Dronning Maud Land, with a significant
394 proportion of the trajectories reaching our study area. In contrast, four out of the six ice core
395 sites used in Goosse et al. (2021) fall outside the primary sink of these trajectories (Fig. 5).
396 This difference in site selection could be a major reason for the observed discrepancy between
397 the two polynya indices. Ice cores from sites that rarely receive air masses from the polynya
398 region may not be reliably used to reconstruct polynya events or may do so with reduced
399 sensitivity. Whereas our ice core site is well located to capture the occurrence of the MRP
400 opening, as it frequently receives air masses originating from the polynya region. However,
401 they still manage to detect the large, multi-year polynyas as they lead to a widespread positive
402 anomaly in precipitation over the coastal and continental region. Another possible reason for
403 this observed difference in sensitivity could be the robustness of our multiproxy approach in
404 identifying polynyas, as it is less susceptible to noise or artefacts in any single proxy. It is
405 crucial to note that the observed differences in peak occurrences do not necessarily invalidate
406 either dataset but rather highlight the complexity in reconstructing past polynya activity. These
407 discrepancies underscore the challenges inherent in paleoclimate reconstruction and the
408 potential complementarity of different methodologies in building a comprehensive
409 understanding of past polynya dynamics.

410 **4.2. Historical polynya activity and its link to maritime climate**

411 Our polynya reconstruction aligns with and extends satellite era observations of MRP
412 formation mechanisms. Recent studies have shed light on the complex interplay of oceanic and
413 atmospheric factors controlling MRP formation and persistence (Campbell et al., 2019; Jena et
414 al., 2019). However, extending these insights to longer timescales remains challenging. Our
415 multi-century reconstruction offers a unique opportunity to explore the long-term drivers of
416 MRP variability. Autonomous profiling float observations during 2016 and 2017 revealed that
417 the MRP were initiated and modulated by the passage of severe storms, and the intense heat
418 loss drove deep overturning within them (Campbell et al., 2019). Wind-driven upwelling of
419 record strength weakened haline stratification in the upper ocean, thus favouring
420 destabilisation. A recent study, however, highlighted the role of salt transport through
421 northward Ekman transport as an additional mechanism of the polynya formation and these
422 processes were driven by intensified eastward surface stresses during 2015 – 2018 (Narayanan
423 et al., 2024).



424 To investigate these factors during the past polynya openings, we used ocean reanalysis
425 outputs from the Simple Ocean Data Assimilation (SODA) version 2.2.4, which spans the
426 period from 1871 to 2010 (Carton and Giese, 2008; Giese and Ray, 2011). It is forced using
427 data assimilation of in-situ temperature and salinity profiles and in-situ and satellite SSTs. This
428 long-term dataset provides monthly fields of ocean temperature, salinity, currents, and sea
429 surface height at a horizontal resolution of $\sim 0.5^\circ$, making it particularly suited for studying
430 large-scale oceanic features and their variability over decadal time scales. Our analysis reveals
431 that periods with high likelihood of polynya occurrences are consistently characterised by
432 increased eastward zonal wind stress due to westerly wind, enhanced northward water flow,
433 and elevated sea surface salinity (Fig. 9). This consistency lends credence to current theories
434 of MRP formation mechanisms and suggests that similar processes operate on multi-decadal
435 to centennial timescales. However, we also observed multiple periods of increased meridional
436 velocity, zonal wind stress, and sea surface salinity that did not invariably lead to a high
437 likelihood of polynya occurrence. This non-linearity underscores the complexity of polynya
438 formation processes and suggests the existence of critical thresholds in wind stress, ocean
439 circulation, or stratification that must be exceeded for polynya formation to occur. The
440 temporal sequencing and duration of favourable conditions also play crucial roles in polynya
441 initiation and maintenance. It could also mean that there are still one or more unexplored
442 processes that control the opening of major polynyas in the Weddell Sea. Our multiproxy
443 approach, combining snow accumulation, water isotopes, and major ion concentrations,
444 provides a more robust reconstruction of polynya activity compared to single-proxy studies.
445 This approach allows us to capture diverse signatures of polynya events and mitigate the
446 limitations of individual proxies.

447 Although beyond the scope of this study, it is crucial to understand the maritime climate
448 variability during the polynya and non-polynya years. Our reconstruction shows alternation
449 between polynya-active and quiescent periods, which may provide valuable context for
450 assessing how future MRP behaviour may evolve under anthropogenic climate change. The
451 clustering of MRPs in our record possibly indicates that once favourable preconditioning
452 develops, the region remains susceptible to repeated polynya openings over several years or
453 decades. As global temperatures rise, projected changes in Southern Ocean wind patterns, sea-
454 ice extent, and surface freshening may shift the thresholds required for deep convection,
455 thereby altering both the frequency and persistence of MRPs. Understanding how atmospheric



456 and oceanic conditions differ between the polynya and non-polynya periods identified in this
457 study will be critical for refining projections. Integrating these insights with high-resolution
458 coupled ocean–atmosphere models could help identify the physical thresholds and feedbacks
459 governing MRP formation. Such integration is crucial for predicting how rare but climatically
460 significant features such as the Maud Rise Polynya may influence Southern Ocean overturning,
461 carbon exchange, and global climate in a warming world.

462 **5. Conclusions and Outlook**

463 We provide new insights into the temporal variability of Maud Rise Polynya, one of
464 the largest and well-known open ocean polynya, by integrating multiple proxies using an ice
465 core from coastal Dronning Maud Land, representing the past nearly 250 years. We identified
466 multiple polynya openings during the 1830s, 1880s, and 1970s. These clusters of polynya
467 openings possibly correspond to a specific combination of atmospheric circulation patterns and
468 oceanographic preconditioning, suggesting a more deterministic framework for MRP
469 development. Over the 250-year record, we identify large events during 1833 – 34 and 1911,
470 which were comparable in magnitude to the documented 1974–1976 polynya, indicating that
471 such openings are not isolated anomalies but represent recurring features of the Southern Ocean
472 system. These events are characterised by proxy signatures consistent with modern polynya
473 conditions, supporting the persistence of underlying formation mechanisms throughout the
474 observational period. Conversely, the interval from 1920 to 1950, marked by a notable absence
475 of polynya activity, coincides with documented changes in Southern Ocean circulation and
476 atmospheric forcing. This prolonged quiescent phase provides valuable baseline information
477 for assessing natural variability in MRP activity on multi-decadal timescales.

478 Our multiproxy approach significantly enhances the sensitivity of the reconstruction,
479 particularly in detecting smaller-magnitude and shorter-duration events that may have been
480 overlooked in previous studies. As a result, the reconstructed history reveals a more dynamic
481 and variable pattern of MRP activity than previously recognised, with implications for
482 understanding its role in ocean ventilation, carbon cycling, and regional climate variability.
483 Our study reveals that synthesising paleoclimate records, modern observations, and modelling
484 approaches can provide a robust foundation for advancing the understanding of the MRP as a
485 critical and recurrent component of the Southern Ocean climate system.



486 **Acknowledgements**

487 The ice core was drilled as part of the India–Norway MADICE project, with support from the
488 Ministry of Earth Sciences, Government of India, and the Research Council of Norway. Ice
489 core drilling and field expeditions have been made successful with the support of the NCPOR
490 logistics leaders, the Maitri logistics team, and all field participants. K. Mahalinganathan and
491 Tariq Ejaz are acknowledged for their contributions to ice core processing and analysis. We
492 acknowledge the use of imagery from the NASA Worldview application
493 (<https://worldview.earthdata.nasa.gov>), part of the NASA Earth Science Data and Information
494 System (ESDIS).

495 **Financial support**

496 This research has been supported by the Ministry of Earth Sciences, India (grant no.
497 MoES/Indo-Nor/PS-3/2015) and the Research Council of Norway (grant no. 248780) for the
498 joint India–Norway project, ‘Mass balance, dynamics, and climate of the central Dronning
499 Maud Land coast, East Antarctica’ (MADICE).

500 **Author contributions**

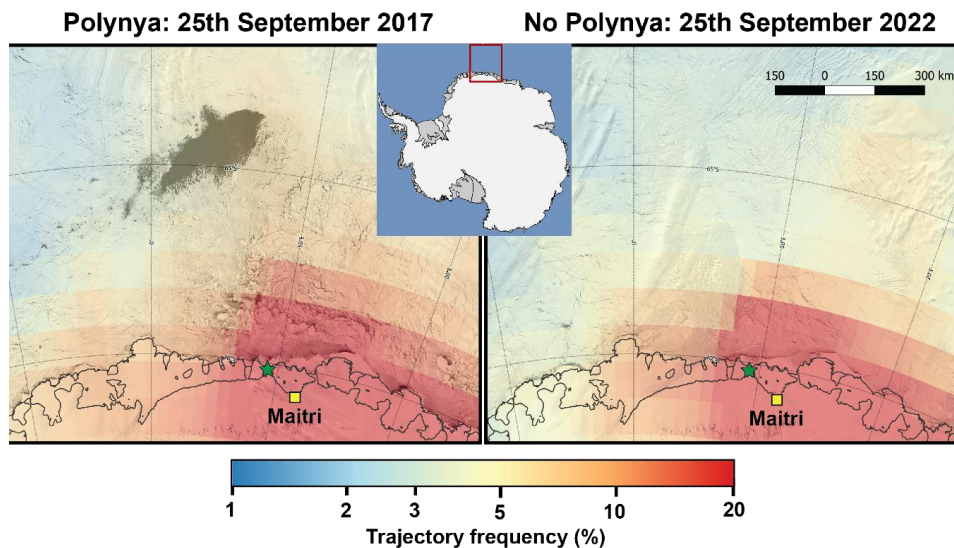
501 RD and MT defined the study objectives. RD led the ice core processing and analysis with
502 support from AP, BLR and CML. RD led the data analysis and interpretation with inputs from
503 KM and CML. RD prepared the manuscript with feedback from all co-authors. MT and KM
504 were the project leaders

505 **Data Availability**

506 All ice core data and polynya indices are being prepared for submission to the NCPOR Polar
507 Data Centre (<https://data.ncpor.res.in>). For final archival, open data formats will be used. A
508 DOI will be generated and included in the final version of the paper. Data access can be granted
509 to reviewers promptly upon request.

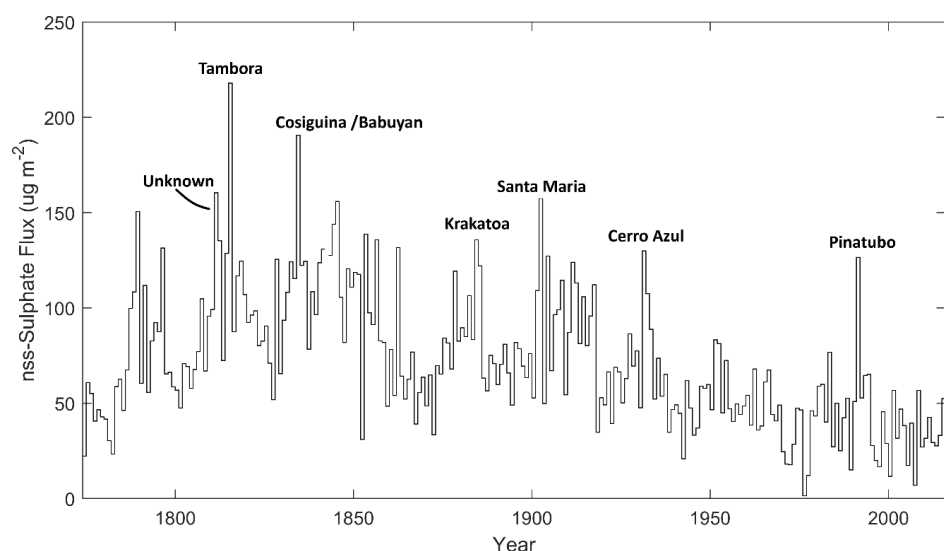
510 **Declaration of competing interest**

511 The authors declare that they have no known competing financial interests or personal
512 relationships that could have appeared to influence the work reported in this paper.



513

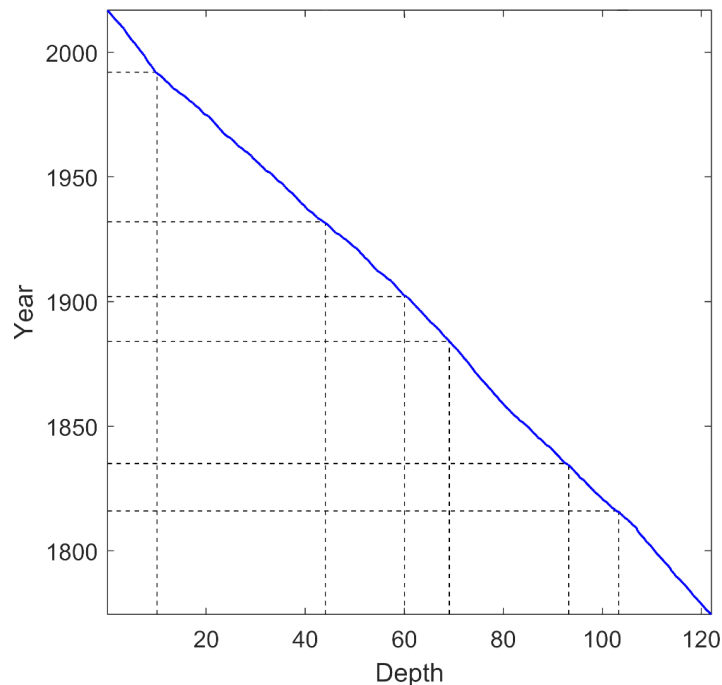
514 **Figure 1 | Study area and wind-trajectory patterns.** (a) Maud Rise Polynya during its largest
515 recent opening on 25 September 2017, detected with Moderate Resolution Imaging
516 Spectroradiometer (MODIS) on NASA's Terra satellite (from NASA Worldview,
517 <https://worldview.earthdata.nasa.gov/>, last access: 15 September 2024). (b) MODIS Satellite
518 imagery taken on the same day in a non-polynya year, 25 September 2022. Images are overlaid
519 with the endpoint frequency of back-trajectories ending at the Djupranen ice core site (green
520 star) from June to October of the years 2017 and 2022, respectively (see methods). The Indian
521 Maitri Station is marked by a yellow square. The colourmap is on a logarithmic scale. The inset
522 shows the location of the main map. Grounding line and calving front are marked (Matsuoka
523 et al., 2015).



524

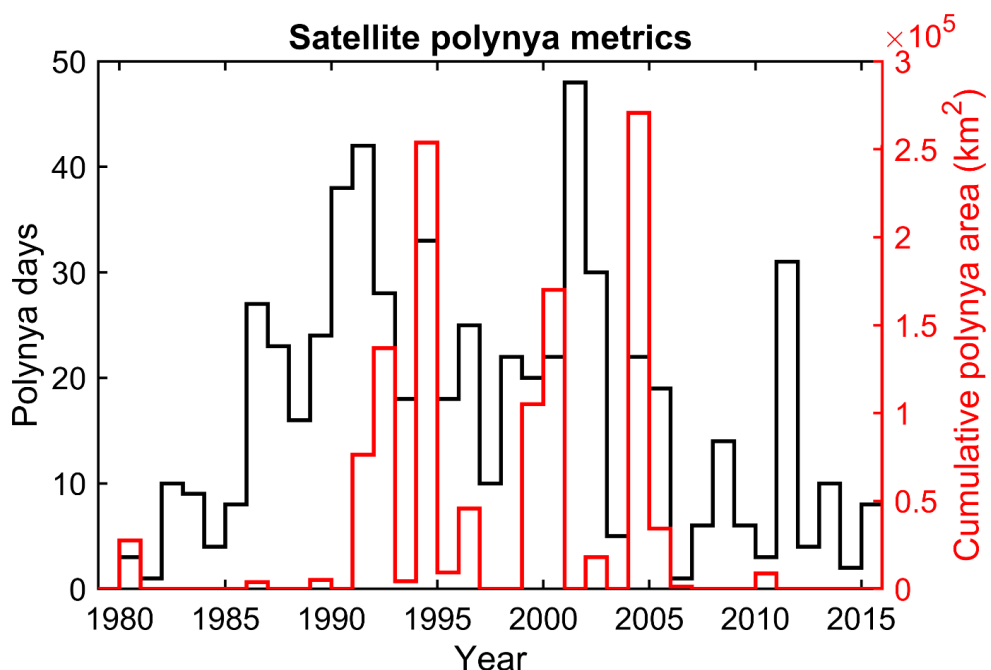
525 **Figure 2 | Tie points for ice core chronology.** Volcanic events are identified from the non-
526 sea-salt sulphate flux records. Only major volcanic events used as age tie points for
527 reconstructing the chronology are marked.

528



529

530 **Figure 3 | Age-depth scale for the Djupranen ice core.** Tie points used for chronology (Fig.
531 2) are shown with dashed lines. Major time markers are shown using the black dashed lines.
532 Minimal deviation from the intersection points of the vertical and horizontal lines indicates the
533 robustness of the chronology.

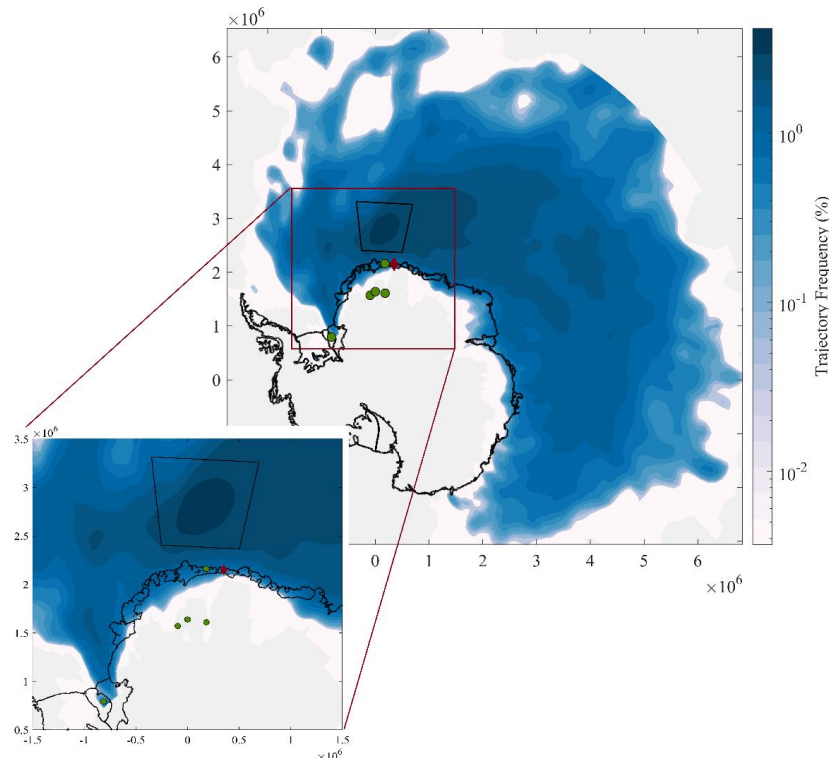


534

535 **Figure 4 | Satellite polynya metrics.** Two different annual metrics of satellite-derived polynya
536 occurrence. Since the polynya is highly dynamic temporally and spatially, the metrics do not
537 show a one-to-one resemblance.



538

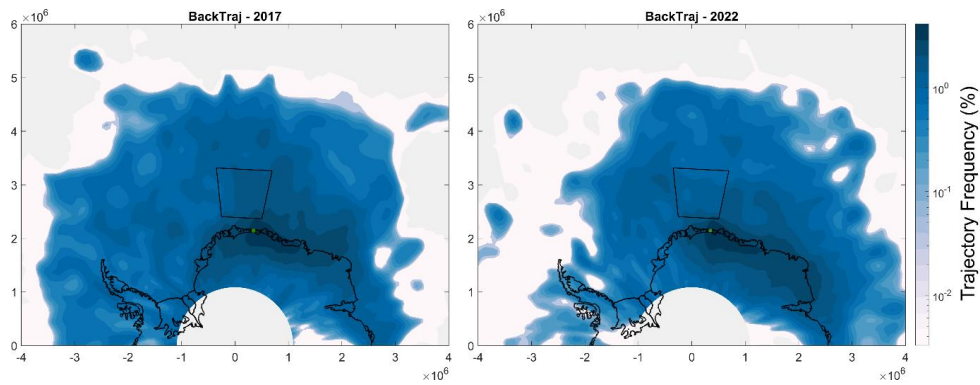


539

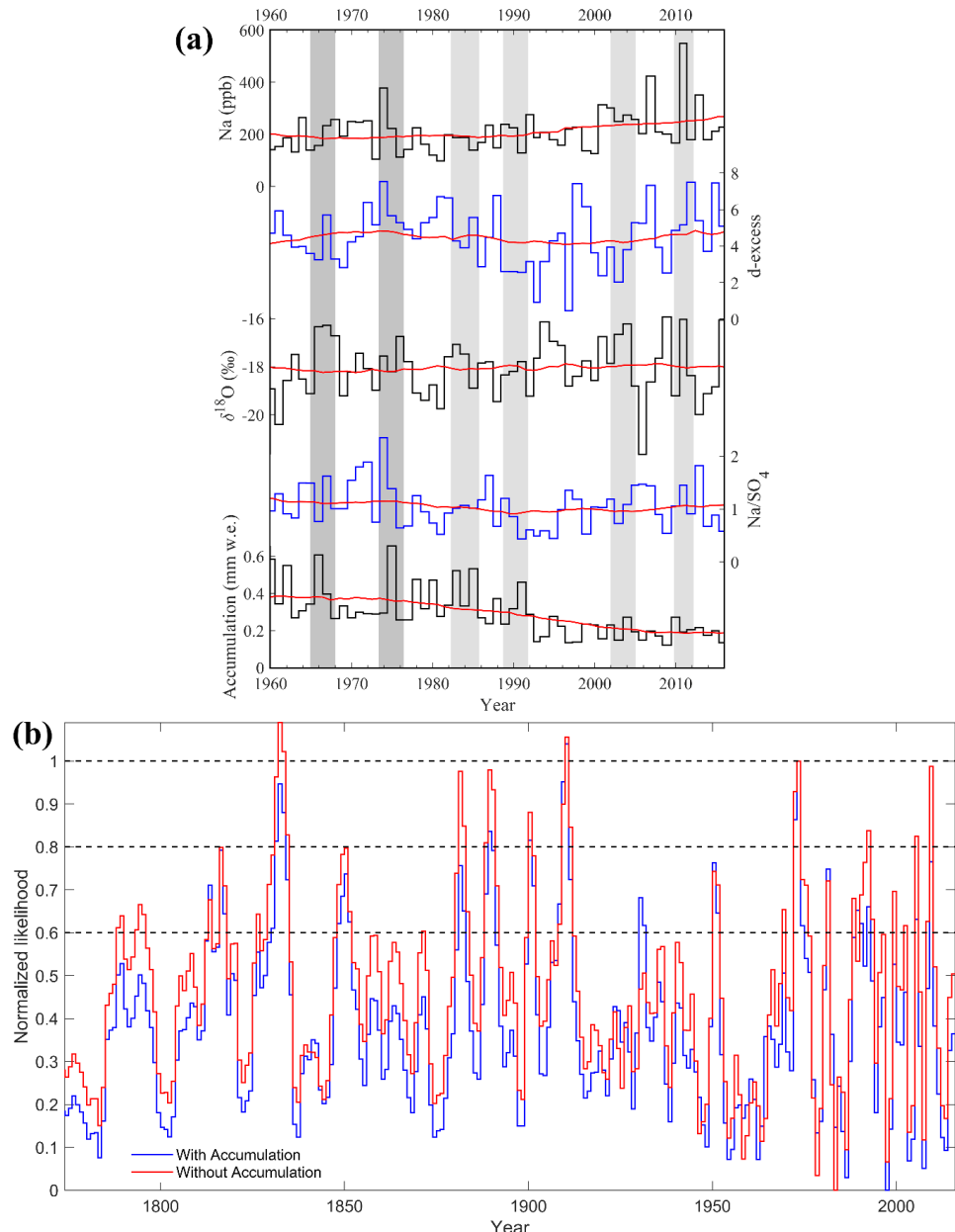
540 **Figure 5 | Airmass transport pathways originating from MRP:** Endpoint frequency of
541 forward trajectories originating over the polynya-prone region (Heuzé et al., 2021) of the
542 Weddell Sea, showing the prevalent transport pathway during the winter to early spring months
543 for the period 1948 – 2016. A significant proportion of the trajectories end over our ice core
544 site (red diamond). Location of ice cores used by Goosse et al., (2021) are shown with green
545 circles. The gray region shows area with no trajectory endpoints.



546



547 **Figure 6 | Airmass transport pathways ending at the ice core site:** Endpoint frequency of
548 back trajectories originating from the ice core site during a well-known polynya year (2017;
549 left) and a non-polynya year (2022; right) is shown. The endpoint frequency pattern during
550 both years is very similar, indicating a consistent transport pathway during most of the years
551 and suggesting that our ice core records activity over the polynya-prone region of the Weddell
552 Sea (black trapezium) in all years. The gray region shows areas with no trajectory endpoints.

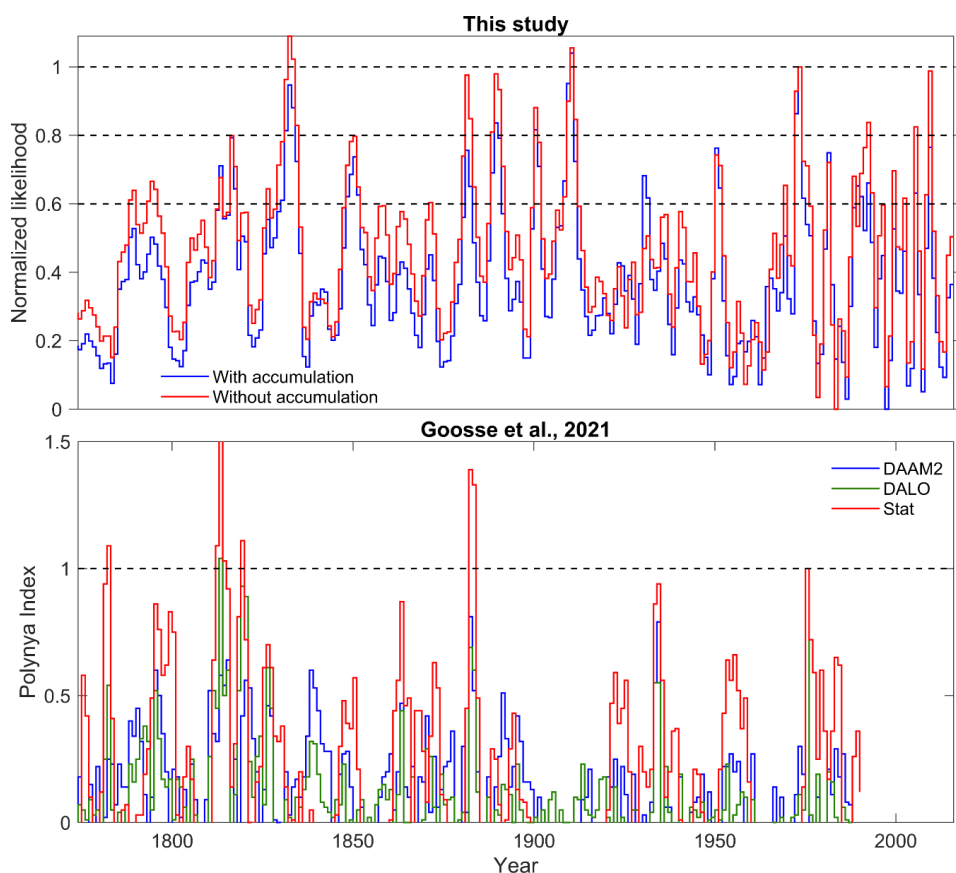


553

554 **Figure 7 | (a) Ice core proxies and polynya identification.** Annual variability of selected ice
 555 core proxy variability from 1960 – 2016. Known events from the satellite data are marked with
 556 dark gray patches for polynya years and light gray patches for halo years (Heuzé et al., 2021).
 557 **(b) Ice core derived polynya indices:** Ice core derived polynya indices in the past 250 years

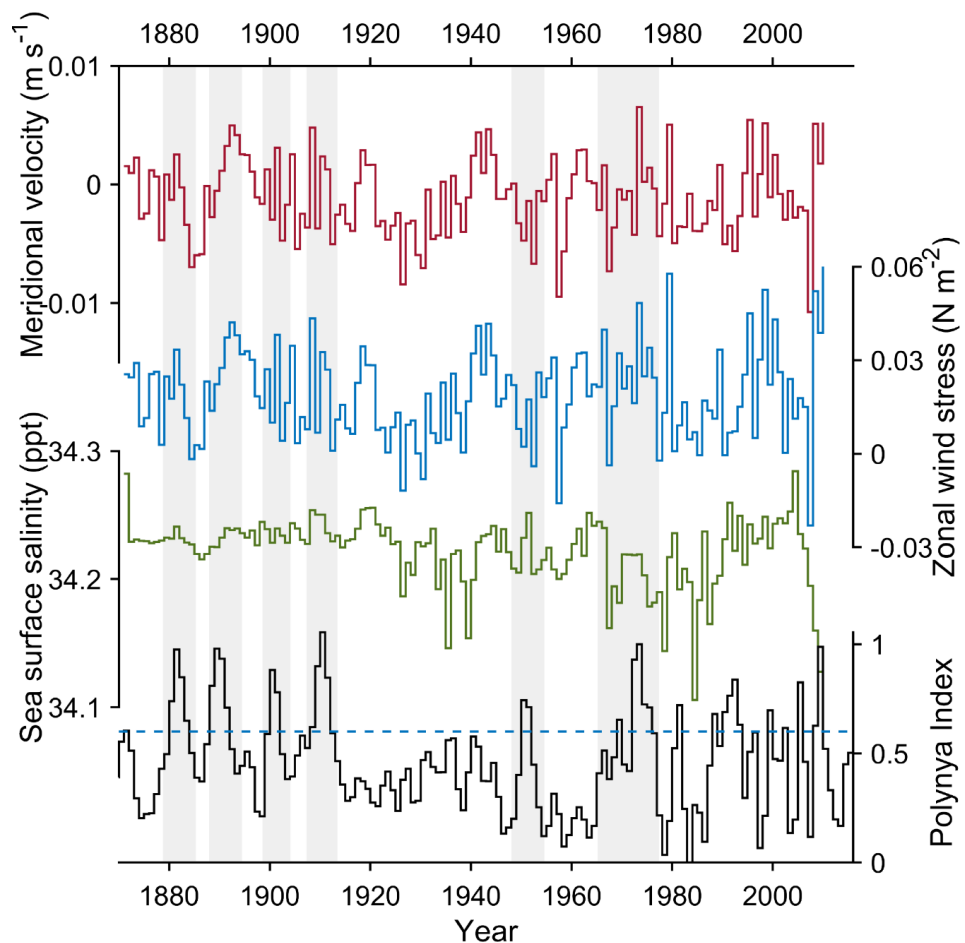


558 using the anomalies in the annual record of five ice-core proxies: Na, deuterium excess, $\delta^{18}\text{O}$,
559 snow accumulation and Na/SO₄ ratio. In order to test the dependence of the polynya index on
560 snow accumulation, we calculate two indices, one using snow accumulation (blue curve) and
561 another without (red curve). The two indices behave similarly over the entire time period;
562 however, the index without snow accumulation shows a higher range of variability. Three
563 different thresholds, 0.6, 0.8, and 1, are set for detecting polynyas.



564

565 **Figure 8 | Comparison of the polynya indices.** Polynya indices reconstructed in this study
566 (upper panel) are shown with the polynya indices from Goosse et al. (2021) (lower panel). The
567 polynya indices from Goosse et al. (2021) are based on six surface mass balance records using
568 data assimilation with two control simulations performed with the SPEAR (Seamless system
569 for Prediction and EArth system Research) global climate model, SPEAR_AM2 (DAAM2;
570 Blue) and SPEAR_LO (DALO; green), and a simple average of the standardized time series
571 (Stat, red).



572

573 **Figure 9 | Factors influencing polynya formations** (a) Mean meridional velocity, (b) zonal
574 wind stress, and (c) sea surface salinity record over the polynya-prone region of the Weddell
575 Sea. (d) Polynya index reconstructed in this study. Grey bars are the major polynya events prior
576 to 1976.



577 References

578 Akitomo, K.: Thermobaric deep convection, baroclinic instability, and their roles in vertical heat
579 transport around Maud Rise in the Weddell Sea, *Journal of Geophysical Research: Oceans*, 111,
580 2006.

581 Arrigo, K. R. and van Dijken, G. L.: Phytoplankton dynamics within 37 Antarctic coastal polynya
582 systems, *Journal of Geophysical Research: Oceans*, 108, 2003.

583 Årthun, M., Holland, P. R., Nicholls, K. W., and Feltham, D. L.: Eddy-Driven Exchange between the
584 Open Ocean and a Sub-Ice Shelf Cavity, *Journal of Physical Oceanography*, 43, 2372-2387,
585 2013.

586 Bennetts, L. G., Shakespeare, C. J., Vreugdenhil, C. A., Foppert, A., Gayen, B., Meyer, A., Morrison,
587 A. K., Padman, L., Phillips, H. E., Stevens, C. L., Toffoli, A., Constantinou, N. C., Cusack, J.
588 M., Cyriac, A., Doddridge, E. W., England, M. H., Evans, D. G., Heil, P., Hogg, A. M., Holmes,
589 R. M., Huneke, W. G. C., Jones, N. L., Keating, S. R., Kiss, A. E., Kraitzman, N., Malyarenko,
590 A., McConnochie, C. D., Meucci, A., Montiel, F., Neme, J., Nikurashin, M., Patel, R. S., Peng,
591 J.-P., Rayson, M., Rosevear, M. G., Sohail, T., Spence, P., and Stanley, G. J.: Closing the Loops
592 on Southern Ocean Dynamics: From the Circumpolar Current to Ice Shelves and From Bottom
593 Mixing to Surface Waves, *Reviews of Geophysics*, 62, e2022RG000781, 2024.

594 Berman, E. S. F., Levin, N. E., Landais, A., Li, S., and Owano, T.: Measurement of $\delta^{18}\text{O}$, $\delta^{17}\text{O}$, and
595 ^{17}O -excess in Water by Off-Axis Integrated Cavity Output Spectroscopy and Isotope Ratio Mass
596 Spectrometry, *Analytical Chemistry*, 85, 10392-10398, 2013.

597 Campbell, E. C., Wilson, E. A., Moore, G. W. K., Riser, S. C., Brayton, C. E., Mazloff, M. R., and
598 Talley, L. D.: Antarctic offshore polynyas linked to Southern Hemisphere climate anomalies,
599 *Nature*, 570, 319-325, 2019.

600 Carsey, F. D.: Microwave Observation of the Weddell Polynya, *Monthly Weather Review*, 108, 2032-
601 2044, 1980.

602 Carton, J. A. and Giese, B. S.: A Reanalysis of Ocean Climate Using Simple Ocean Data Assimilation
603 (SODA), *Monthly Weather Review*, 136, 2999-3017, 2008.

604 Comiso, J. C. and Gordon, A. L.: Recurring polynyas over the Cosmonaut Sea and the Maud Rise,
605 *Journal of Geophysical Research: Oceans*, 92, 2819-2833, 1987.

606 Comiso, J. C. and Nishio, F.: Trends in the sea ice cover using enhanced and compatible AMSR-E,
607 SSM/I, and SMMR data, *Journal of Geophysical Research: Oceans*, 113, 2008.

608 de Lavergne, C., Palter, J. B., Galbraith, E. D., Bernardello, R., and Marinov, I.: Cessation of deep
609 convection in the open Southern Ocean under anthropogenic climate change, *Nature Climate
610 Change*, 4, 278-282, 2014.

611 Dey, R.: Reconstruction of Antarctic climate variability using high resolution ice core stratigraphy,
612 2023. Goa University, 2023.

613 Dey, R., Thamban, M., Laluraj, C. M., Mahalinganathan, K., Redkar, B. L., Kumar, S., and Matsuoka,
614 K.: Application of visual stratigraphy from line-scan images to constrain chronology and melt
615 features of a firn core from coastal Antarctica, *Journal of Glaciology*, 69, 179-190, 2023.



616 Dixon, D. A., Mayewski, P. A., Goodwin, I. D., Marshall, G. J., Freeman, R., Maasch, K. A., and Snead,
617 S. B.: An ice-core proxy for northerly air mass incursions into West Antarctica, International
618 Journal of Climatology, 32, 1455-1465, 2012.

619 Dorling, S. R. and Davies, T. D.: Extending cluster analysis—synoptic meteorology links to
620 characterise chemical climates at six northwest European monitoring stations, Atmospheric
621 Environment, 29, 145-167, 1995.

622 Draxler, R.: NOAA-Air resources laboratory-FAQ-How do i estimate the absolute (in km) and relative
623 (%) errors when using the HYSPLIT trajectory model. Sept, 2008.

624 Drews, R., Matsuoka, K., Martín, C., Callens, D., Bergeot, N., and Pattyn, F.: Evolution of Derwael Ice
625 Rise in Dronning Maud Land, Antarctica, over the last millennia, Journal of Geophysical
626 Research: Earth Surface, 120, 564-579, 2015.

627 Ejaz, T., Rahaman, W., Laluraj, C. M., Mahalinganathan, K., and Thamban, M.: Rapid Warming Over
628 East Antarctica Since the 1940s Caused by Increasing Influence of El Niño Southern Oscillation
629 and Southern Annular Mode, Frontiers in Earth Science, Volume 10 - 2022, 2022.

630 Ejaz, T., Rahaman, W., Laluraj, C. M., Mahalinganathan, K., and Thamban, M.: Sea Ice Variability and
631 Trends in the Western Indian Ocean Sector of Antarctica During the Past Two Centuries and Its
632 Response to Climatic Modes, Journal of Geophysical Research: Atmospheres, 126,
633 e2020JD033943, 2021.

634 Giese, B. S. and Ray, S.: El Niño variability in simple ocean data assimilation (SODA), 1871–2008,
635 Journal of Geophysical Research: Oceans, 116, 2011.

636 Goel, V., Brown, J., and Matsuoka, K.: Glaciological settings and recent mass balance of Blåskimen
637 Island in Dronning Maud Land, Antarctica, The Cryosphere, 11, 2883-2896, 2017.

638 Goel, V., Matsuoka, K., Berger, C. D., Lee, I., Dall, J., and Forsberg, R.: Characteristics of ice rises and
639 ice rumples in Dronning Maud Land and Enderby Land, Antarctica, Journal of Glaciology, 66,
640 1064-1078, 2020.

641 Goosse, H., Dalaïden, Q., Cavitte, M. G. P., and Zhang, L.: Can we reconstruct the formation of large
642 open-ocean polynyas in the Southern Ocean using ice core records?, Clim. Past, 17, 111-131,
643 2021.

644 Gordon, A. L. and Comiso, J. C.: Polynyas in the Southern Ocean, Scientific American, 258, 90-97,
645 1988.

646 Goursaud, S., Masson-Delmotte, V., Favier, V., Preunkert, S., Fily, M., Gallée, H., Jourdain, B.,
647 Legrand, M., Magand, O., Minster, B., and Werner, M.: A 60-year ice-core record of regional
648 climate from Adélie Land, coastal Antarctica, The Cryosphere, 11, 343-362, 2017.

649 Gülk, B., Roquet, F., Naveira Garabato, A. C., Bourdallé-Badie, R., Madec, G., and Giordani, H.:
650 Impacts of Vertical Convective Mixing Schemes and Freshwater Forcing on the 2016–2017
651 Maud Rise Polynya Openings in a Regional Ocean Simulation, Journal of Advances in Modeling
652 Earth Systems, 16, e2023MS004106, 2024.

653 Heuzé, C., Heywood, K. J., Stevens, D. P., and Ridley, J. K.: Southern Ocean bottom water
654 characteristics in CMIP5 models, Geophysical Research Letters, 40, 1409-1414, 2013.

655 Heuzé, C., Zhou, L., Mohrmann, M., and Lemos, A.: Spaceborne infrared imagery for early detection



656 of Weddell Polynya opening, *The Cryosphere*, 15, 3401-3421, 2021.

657 Holland, D. M.: Explaining the Weddell Polynya--a Large Ocean Eddy Shed at Maud Rise, *Science*,
658 292, 1697-1700, 2001.

659 Jacobs, S. S., Gordon, A. L., and Ardal, J. L.: Circulation and Melting Beneath the Ross Ice Shelf,
660 *Science*, 203, 439-443, 1979.

661 Jena, B., Ravichandran, M., and Turner, J.: Recent Reoccurrence of Large Open-Ocean Polynya on the
662 Maud Rise Seamount, *Geophysical Research Letters*, 46, 4320-4329, 2019.

663 Jones, T. R., Cuffey, K. M., Roberts, W. H. G., Markle, B. R., Steig, E. J., Stevens, C. M., Valdes, P.
664 J., Fudge, T. J., Sigl, M., Hughes, A. G., Morris, V., Vaughn, B. H., Garland, J., Vinther, B. M.,
665 Rozmiarek, K. S., Brashears, C. A., and White, J. W. C.: Seasonal temperatures in West Antarctica
666 during the Holocene, *Nature*, 613, 292-297, 2023.

667 Klein, F., Abram, N. J., Curran, M. A. J., Goosse, H., Goursaud, S., Masson-Delmotte, V., Moy, A.,
668 Neukom, R., Orsi, A., Sjolte, J., Steiger, N., Stenni, B., and Werner, M.: Assessing the robustness
669 of Antarctic temperature reconstructions over the past 2 millennia using pseudoproxy and data
670 assimilation experiments, *Clim. Past*, 15, 661-684, 2019.

671 Lenaerts, J. T. M., Brown, J., Van Den Broeke, M. R., Matsuoka, K., Drews, R., Callens, D., Philippe,
672 M., Gorodetskaya, I. V., Van Meijgaard, E., Reijmer, C. H., Pattyn, F., and Van Lipzig, N. P. M.:
673 High variability of climate and surface mass balance induced by Antarctic ice rises, *Journal of
674 Glaciology*, 60, 1101-1110, 2014.

675 Levine, J. G., Yang, X., Jones, A. E., and Wolff, E. W.: Sea salt as an ice core proxy for past sea ice
676 extent: A process-based model study, *Journal of Geophysical Research: Atmospheres*, 119, 5737-
677 5756, 2014.

678 Lindsay, R. W., Holland, D. M., and Woodgate, R. A.: Halo of low ice concentration observed over the
679 Maud Rise seamount, *Geophysical Research Letters*, 31, 2004.

680 Markle, B. R., Bertler, N. A. N., Sinclair, K. E., and Sneed, S. B.: Synoptic variability in the Ross Sea
681 region, Antarctica, as seen from back-trajectory modeling and ice core analysis, *Journal of
682 Geophysical Research: Atmospheres*, 117, 2012.

683 Matsuoka, K., Hindmarsh, R. C. A., Moholdt, G., Bentley, M. J., Pritchard, H. D., Brown, J., Conway,
684 H., Drews, R., Durand, G., Goldberg, D., Hattermann, T., Kingslake, J., Lenaerts, J. T. M.,
685 Martín, C., Mulvaney, R., Nicholls, K. W., Pattyn, F., Ross, N., Scambos, T., and Whitehouse,
686 P. L.: Antarctic ice rises and ripples: Their properties and significance for ice-sheet dynamics
687 and evolution, *Earth-Science Reviews*, 150, 724-745, 2015.

688 McHedlishvili, A., Spreen, G., Melsheimer, C., and Huntemann, M.: Weddell Sea polynya analysis
689 using SMOS-SMAP apparent sea ice thickness retrieval, *The Cryosphere*, 16, 471-487, 2022.

690 McPhee, M. G.: Is thermobaricity a major factor in Southern Ocean ventilation?, *Antarctic Science*, 15,
691 153-160, 2003.

692 Meier, W. N., Gallaher, D., and Campbell, G. G.: New estimates of Arctic and Antarctic sea ice extent
693 during September 1964 from recovered Nimbus I satellite imagery, *The Cryosphere*, 7, 699-705,
694 2013.

695 Moore, G. W. K., Alverson, K., and Renfrew, I. A.: A Reconstruction of the Air-Sea Interaction



696 Associated with the Weddell Polynya, *Journal of Physical Oceanography*, 32, 1685-1698, 2002.

697 698 699 700 Naik, S. S., Thamban, M., Laluraj, C. M., Redkar, B. L., and Chaturvedi, A.: A century of climate variability in central Dronning Maud Land, East Antarctica, and its relation to Southern Annular Mode and El Niño-Southern Oscillation, *Journal of Geophysical Research: Atmospheres*, 115, 2010.

701 702 703 Narayanan, A., Roquet, F., Gille, S. T., Gulk, B., Mazloff, M. R., Silvano, A., and Naveira Garabato, A. C.: Ekman-driven salt transport as a key mechanism for open-ocean polynya formation at Maud Rise, *Science Advances*, 10, eadj0777, 2024.

704 705 Neff, P. D. and Bertler, N. A. N.: Trajectory modeling of modern dust transport to the Southern Ocean and Antarctica, *Journal of Geophysical Research: Atmospheres*, 120, 9303-9322, 2015.

706 707 708 709 Philippe, M., Tison, J. L., Fjøsne, K., Hubbard, B., Kjær, H. A., Lenaerts, J. T. M., Drews, R., Sheldon, S. G., De Bondt, K., Claeys, P., and Pattyn, F.: Ice core evidence for a 20th century increase in surface mass balance in coastal Dronning Maud Land, East Antarctica, *The Cryosphere*, 10, 2501-2516, 2016.

710 711 712 Pratap, B., Dey, R., Matsuoka, K., Moholdt, G., Lindbäck, K., Goel, V., Laluraj, C. M., and Thamban, M.: Three-decade spatial patterns in surface mass balance of the Nivlisen Ice Shelf, central Dronning Maud Land, East Antarctica, *Journal of Glaciology*, 68, 174-186, 2022.

713 714 Richardson, C.: Phase Relationships in Sea Ice as a Function of Temperature, *Journal of Glaciology*, 17, 507-519, 1976.

715 716 717 Rignot, E., Mouginot, J., Scheuchl, B., van den Broeke, M., van Wessem, M. J., and Morlighem, M.: Four decades of Antarctic Ice Sheet mass balance from 1979–2017, *Proceedings of the National Academy of Sciences*, 116, 1095-1103, 2019.

718 719 720 721 Sallée, J.-B., Shuckburgh, E., Bruneau, N., Meijers, A. J. S., Bracegirdle, T. J., Wang, Z., and Roy, T.: Assessment of Southern Ocean water mass circulation and characteristics in CMIP5 models: Historical bias and forcing response, *Journal of Geophysical Research: Oceans*, 118, 1830-1844, 2013.

722 The Firn Symposium team: Firn on ice sheets, *Nature Reviews Earth & Environment*, 5, 79-99, 2024.

723 724 725 The SO-CHIC consortium: Southern ocean carbon and heat impact on climate, *Philosophical Transactions of the Royal Society A: Mathematical, Physical and Engineering Sciences*, 381, 20220056, 2023.

726 727 Visbeck, M., Marshall, J., and Jones, H.: Dynamics of Isolated Convective Regions in the Ocean, *Journal of Physical Oceanography*, 26, 1721-1734, 1996.

728 729 730 Wagenbach, D., Ducroz, F., Mulvaney, R., Keck, L., Minikin, A., Legrand, M., Hall, J. S., and Wolff, E. W.: Sea-salt aerosol in coastal Antarctic regions, *Journal of Geophysical Research: Atmospheres*, 103, 10961-10974, 1998.

731 732 733 Wauthy, S., Tison, J. L., Inoue, M., El Amri, S., Sun, S., Fripiat, F., Claeys, P., and Pattyn, F.: Spatial and temporal variability of environmental proxies from the top 120 m of two ice cores in Dronning Maud Land (East Antarctica), *Earth Syst. Sci. Data*, 16, 35-58, 2024.

734 735 Wilson, E. A., Riser, S. C., Campbell, E. C., and Wong, A. P. S.: Winter Upper-Ocean Stability and Ice–Ocean Feedbacks in the Sea Ice–Covered Southern Ocean, *Journal of Physical*



736 Oceanography, 49, 1099-1117, 2019.

737 Winstrup, M., Svensson, A. M., Rasmussen, S. O., Winther, O., Steig, E. J., and Axelrod, A. E.: An
738 automated approach for annual layer counting in ice cores, *Clim. Past*, 8, 1881-1895, 2012.

739 Wolff, E. W., Rankin, A. M., and Röthlisberger, R.: An ice core indicator of Antarctic sea ice
740 production?, *Geophysical Research Letters*, 30, 2003.

741 Xu, Y., Zhang, W., Maksym, T., Ji, R., and Li, Y.: Stratification Breakdown in Antarctic Coastal
742 Polynyas. Part I: Influence of Physical Factors on the Destratification Time Scale, *Journal of*
743 *Physical Oceanography*, 53, 2047-2067, 2023.

744 Zheng, W. E. I., Zhaoru, Z., Timo, V., Xiaoqiao, W., and Yuanjie, C.: An overview of Antarctic
745 polynyas: sea ice production, forcing mechanisms, temporal variability and water mass
746 formation, *Advances in Polar Science*, 32, 295-311, 2021.

747 Zhou, L., Heuzé, C., and Mohrmann, M.: Sea Ice Production in the 2016 and 2017 Maud Rise Polynyas,
748 *Journal of Geophysical Research: Oceans*, 128, e2022JC019148, 2023.

749 Zwally, H. J., Comiso, J. C., and Gordon, A. L.: Antarctic Offshore Leads and Polynyas and
750 Oceanographic Effects. In: *Oceanology of the Antarctic Continental Shelf*, 1985.

751